1   REVISION 1

2   Abstract + Main Text Word count: 5790

3   **Bobfinchite, Na[(UO$_2$)$_8$O$_3$(OH)$_{11}$]·10H$_2$O, a new Na-bearing**

4   **member of the schoepite family**

5   Travis A. Olds[1*], Jakub Plášil[2], Anthony R. Kampf[3], Peter C. Burns[4,5], Joe
6   Marty[6], John S. McCloy[7]
7
8   [1] Section of Minerals & Earth Sciences, Carnegie Museum of Natural History,
9   4400 Forbes Avenue, Pittsburgh, Pennsylvania 15213, USA
10   [2] Institute of Physics ASCR, v.v.i., Na Slovance 1999/2, 18221 Prague 8,
11   Czech Republic
12   [3] Mineral Sciences Department, Natural History Museum of Los Angeles
13   County, 900 Exposition Boulevard, Los Angeles, CA 90007, USA
14   [4] Department of Civil and Environmental Engineering and Earth Sciences,
15   University of Notre Dame, Notre Dame, IN 46556, USA
16   [5] Department of Chemistry and Biochemistry, University of Notre Dame,
17   Notre Dame, IN 46556, USA
18   [6] 5199 East Silver Oak Road, Salt Lake City, UT 84108, USA
19   [7] School of Mechanical and Materials Engineering, Washington State
20   University, Pullman, WA, 99163, USA
21
22   *E-mail: oldst@carnegiemnh.org

23   **Abstract**

24   The new mineral bobfinchite (IMA2020–082),

25   Na[(UO$_2$)$_8$O$_3$(OH)$_{11}$]·10H$_2$O, was found in the Burro mine, Slick Rock

26   district, San Miguel County, Colorado, USA, where it occurs as an oxidation

27   product of uraninite on asphaltite matrix in intimate association with gypsum,

28   natrozippeite, metaschoepite, and uranopilite. Bobfinchite crystals are

29   transparent to translucent, yellow, lozenge-shaped discs up to 0.3 mm wide.

30   Crystals are flattened on [100] and exhibit the forms {100}, {011}, {021}, {0-

31   21}, and {0-11}. Bobfinchite has a pale-yellow streak and emits very dim

32   yellow fluorescence under 365 nm ultraviolet illumination. The crystals are

33   brittle with very good {100} cleavage and irregular, stepped fracture. The

34 Mohs hardness is *ca.* 2 based on scratch tests. The calculated density is 5.044

35 $g \cdot cm^{-3}$ based on the empirical formula and 5.036 $g \cdot cm^{-3}$ for the ideal formula.

36 Bobfinchite is optically biaxial (–), with $\alpha = 1.690(5)$, $\beta = 1.7205(5)$, and $\gamma =$

37 1.730(5) (white light). The measured 2V, estimated from the interference

38 figure, is 55(5)° and the calculated value is 59.1°. Dispersion is moderate, $r >$

39 v; orientation: $X = $ **a**, $Y = $ **b**, $Z = $ **c**; pleochroism: X nearly colourless, Y yellow,

40 Z yellow; $X < Y \approx Z$. Electron microprobe analysis provided the empirical

41 formula $(Na_{0.99}Pb_{0.02})[(UO_2)_{7.99}O_3(OH)_{11}] \cdot 10H_2O$. The five strongest X-ray

42 powder diffraction lines are [d_{obs} Å(I)(hkl)]: 7.34(100)(200), 3.59(50)(024),

43 3.23(60)(224), 3.18(36)(240) and 2.01(23)(624,551,208,640,346). Bobfinchite

44 is orthorhombic, *Pbcn*, $a = 14.6249(9)$, $b = 14.0389(10)$, $c = 16.6923(10)$ Å, V

45 $= 3427.2(4)$ Å^3 and $Z = 4$. The structure of bobfinchite ($R_1 = 0.0330$ for 3770 I

46 $> 4\sigma I$) is built from uranyl oxide-hydroxide sheets that adopt the fourmarierite

47 topology, with interlayer Na^+ and H_2O groups. Both the sheet and interlayer

48 topology mimic those observed in natural and synthetic Na-metaschoepites

49 studied previously, and as seen in other uranyl oxide hydrate minerals, charge

50 balance is achieved at specific sites in the sheet through the substitution $O^{2-} \Leftrightarrow$

51 $(OH)^-$.

52

53 **Keywords:** New mineral, metaschoepite, schoepite family, uranyl oxide

54 hydrate, X-ray crystallography, Raman spectroscopy

55

56 **Introduction**

57 Uranyl oxide hydrates (UOH) are frequently encountered alteration phases in

58 uranium mines and the technogenic environments of the nuclear fuel cycle

2

59   (Finch and Ewing, 1992; Finch et al., 1992; Finch and Murakami, 1999; Plášil,

60   2014; Plášil, 2018b). UOH minerals crystallize in mines where uranyl-bearing

61    $(UO_2)^{2+}$ solutions created from uraninite (UO_{2+x}) under oxidizing conditions

62   interact with the surrounding rocks and soils. In some instances, later

63   hydrolysis of uranyl minerals (e.g. natrozippeite) can lead to the formation of

64   UOH's like schoepite, metaschoepite, heisenbergite, and paulscherrerite

65   (Brugger et al., 2011). Likewise, UOH and schoepite-family related phases

66   have historically been heavily scrutinized materials in countless experiments

67   related to the engineered environments of the nuclear fuel cycle, where they

68   occur as prevalent products of hydrothermal reactions with used nuclear fuel

69   and other U-rich nuclear materials (Fallon et al., 2023; Giammar and Hering,

70   2004; Gorman-Lewis et al., 2008; Hanson et al., 2005; Riba et al., 2005). The

71   observations made from natural occurrences, laboratory, and field alteration

72   studies involving UOH and schoepite-family minerals reveal intricate

73   dependencies of their formation and stability on local conditions, and that

74   these phases are the dominant solubility-limiting phases produced during the

75   dissolution of uranium dioxide (Colmenero et al., 2019; Knope and

76   Soderholm, 2013; Zhang et al., 2022). The resulting chemical and structural

77   differences found in the U-O-H system leads to a diverse phase space that is

78   primarily time, temperature, hydration state, and radiation-field dependent

79   (Benjamin et al., 2022; Finch et al., 1998; Kirkegaard et al., 2019; Sowder et

80   al., 1999; Sunder et al., 1992; Taylor et al., 1991). We add to this complex and

81   important phase space with the description of bobfinchite, the first Na-bearing

82   member of the schoepite family.

3

83   Bobfinchite is named in honor of American mineralogist and global

84   nuclear security and nonproliferation analyst Robert James Finch (born 1958).

85   Dr. Finch received a Ph.D. in Earth and Planetary Sciences in 1994 from the

86   University of New Mexico for his work on the paragenesis and crystal

87   chemistry of uranyl oxide hydrates. Subsequent to post-doctoral research at

88   the University of Manitoba, in 1996 Bob joined Argonne National Laboratory

89   and performed a variety of research in applied mineralogy that focused on

90   corrosion of spent nuclear fuel under hypothetical repository conditions. He

91   has been involved in the structural description of many uranium minerals and

92   synthetic phases containing uranium, including rutherfordine, ianthinite,

93   billietite, wyartite, and dehydrated wyartite. Bob was the first to determine and

94   refine the structure of schoepite (Finch et al., 1996) and provided the first

95   refinement of the structure of metaschoepite from altered schoepite and the

96   powders produced by heating schoepite (Finch et al., 1998). He has published

97   many articles, conference proceedings, books, and book chapters focused on

98   uranium minerals and nuclear materials, including serving as co-editor and

99   contributor to Uranium: Mineralogy, Geochemistry and the Environment,

100   Reviews in Mineralogy vol. 38, published by the Mineralogical Society of

101   America.

102   The mineral and its name have been approved by the Commission on

103   New Minerals, Nomenclature and Classification of the International

104   Mineralogical Association (IMA2020–082). The holotype specimen deposited

105   in the collections of the Natural History Museum of Los Angeles County, 900

106   Exposition Boulevard, Los Angeles, CA 90007, USA, catalogue number

107   75146.

4

108

Occurrence

109

110   Bobfinchite was found underground in the Burro mine, Slick Rock

111   district, San Miguel County, Colorado, USA (38°2'42"N 108°53'23"W). The

112   Burro mine is located on the southern edge of the Uravan Mineral Belt in

113   southwestern Colorado, where numerous uranium and vanadium mines occur

114   in bedded sandstone and roll-front deposits of the Salt Wash member of the

115   Jurassic Morrison Formation (Carter and Gualtieri, 1965; Shawe, 2011).

116   Uranium and vanadium ores deposited where U- and V-rich solutions

117   encountered regions of reducing solutions that had developed around

118   accumulations of carbonaceous plant material (asphaltite). Post-mining

119   oxidation and leaching of uranyl cations, $(UO_2)^{2+}$, from uraninite embedded in

120   the asphaltite led to the formation of bobfinchite.

121   The new mineral crystallized directly on asphaltite and is intimately

122   associated with other secondary uranyl minerals including natrozippeite,

123   metaschoepite, and uranopilite. Bobfinchite occurs very rarely in the Burro

124   mine, having so far been found in one relatively small pod of asphaltite,

125   measuring approximately 3 feet wide and 8-10 inches thick. Other minerals in

126   close association include abundant gypsum and sporadic tufts of an

127   unidentified and poorly-diffracting fibrous and hydrous mineral containing

128   major U, V, S, and O, with minor Al, P, and Mg. In the same aphaltite pod,

129   but not in close association with bobfinchite, we have identified crystals of

130   uroxite, metauroxite, sklodowskite, and an additional unidentified but poorly

131   crystallized hydrous mineral with a complex and variable composition

132   including U, C, V, S, P, and As.

5

133   Some paragenetic insights can be inferred despite the complex local

134   secondary mineralization. The largest and highest quality bobfinchite crystals

135   were found growing directly on asphaltite, and are commonly overgrown by

136   and intergrown with well-crystallized natrozippeite and uranopilite, suggesting

137   that bobfinchite may have been one of the first secondary minerals formed

138   there, or that it had co-precipitated with these minerals. Associated

139   metaschoepite is generally poorly formed, occurring as anhedral or bubbly

140   aggregates with abundant gypsum in intimate association.

141
142   **Physical and optical properties**

143   Bobfinchite crystals are yellow lozenge-shaped discs occurring as

144   individuals, reaching up to 0.3 mm wide, and as yellow to golden-yellow

145   polycrystalline aggregates up to 0.5 mm wide (Fig. 1). Crystals are flattened

146   on [100] and exhibit the forms {100}, {011}, {021}, {0-21}, {0-11} (Fig. 2).

147   They are transparent to translucent with a vitreous luster, have a pale-yellow

148   streak and extremely dim yellow fluorescence was observed under 365 nm

149   ultraviolet illumination only. The crystals are brittle with very good {100}

150   cleavage and irregular, stepped fracture. The Mohs hardness is about 2 based

151   on scratch tests. The density could not be measured because it exceeds that of

152   available heavy liquids. The calculated density is 5.044 g·cm^{-3} based on the

153   empirical formula and 5.036 g·cm^{-3} for the ideal formula. Bobfinchite is

154   slowly soluble in dilute HCl.

155   Optically, bobfinchite is biaxial (–), with $\alpha = 1.690(5)$, $\beta = 1.7205(5)$,

156   and $\gamma = 1.730(5)$ (measured in white light). The measured $2V$ estimated from

157   the interference figure is 55(5)° and the calculated value is 59.1°. Dispersion is

158   moderate, with $r > v$. The optical orientation is $X = \mathbf{a}$, $Y = \mathbf{b}$, $Z = \mathbf{c}$;

159   pleochroism: X nearly colourless, Y yellow, Z yellow; $X < Y \approx Z$. The

160   Gladstone-Dale compatibility (Mandarino, 2007), $1 - (K_p/K_c)$, is -0.017

161   (superior) for the empirical formula using k = 0.118.

162

163   **Raman Spectroscopy**

164   Raman spectroscopy was conducted using a Thermo Scientific

165   DXR2xi with excitation by a 785 nm laser and detection from 1800-50 cm^{-1}

166   (Fig. 3). The spectrum was taken using a laser output of 10 mW focused onto

167   the sample surface using a 50x objective. The laser was internally calibrated

168   prior to measurement *via* a software controlled (OMNICxi) procedure using

169   neon emission lines (wavelength calibration), polystyrene bands (laser

170   frequency calibration), and a standardized white light source (intensity

171   calibration).

172   We observed no bands related to ν OH vibrations in the high

173   wavenumber region of the spectrum using the 785 nm laser; however, a broad

174   band related to the ν_2 (δ) bending vibrations of H_2O groups is present at 1599

175   cm^{-1}, enveloping a minor component at 1563 cm^{-1} that may be attributed to

176   the same mode, or possibly to a combination band or δ-UOH bending mode.

177   In schoepite, the ν_2 (δ) H_2O band occurs at 1621 cm^{-1}, and density functional

178   perturbation theory (DFPT) calculations of the vibrational properties of

179   schoepite by Colmenero et al. (2018) reveals the presence of two bands at

180   1624 cm^{-1} and 1605 cm^{-1}. The series of broad bands between ~1400 cm^{-1} and

181   1200 cm^{-1} in the spectrum of bobfinchite probably occur due to δ-UOH

182   bending modes, with fitted centers at 1328 cm^{-1}, 1262 cm^{-1}, and 1204 cm^{-1};

183   however, no bands were identified in this region by DFPT calculations of

184   schoepite. Likewise, in the Raman spectrum of synthetic metaschoepite,

185   Kirkegaard et al. (2019) observe no bands above 869 cm^{-1}.

186   Slight nonlinearity of the uranyl bonds in bobfinchite has led to

187   activation of the ν_3 $(UO_2)^{2+}$ antisymmetric stretching vibration, which occurs

188   as a very weak band at 967 cm^{-1}. The ν_1 $(UO_2)^{2+}$ symmetric stretching

189   vibration is present as a strong and complex band; fitting reveals that it is

190   composed of at least seven components with centers at 894, 852, 839, 829,

191   822, 809, and 800 cm^{-1}. These bands likely include contributions from UOH

192   bending vibrations, and although most components in this region were

193   considered as symmetric uranyl stretching vibrations by Frost et al. (2007),

194   DFPT calculations by Colmenero et al. (2018) indicate the bands at 897, 886,

195   870, and 855 cm^{-1} in schoepite correspond to an overlap of UOH bending

196   vibrations and H_2O librations. Bartlett and Cooney (1989) provide an

197   empirical relationship to derive the approximate U-O_{yl} bond lengths from the

198   band positions assigned to the $(UO_2)^{2+}$ stretching vibrations, which gives 1.74

199   Å for ν_3, and for the components correlating with ν_1 assignments by

200   Colmenero (2018): 1.76 Å (852 cm^{-1}), 1.77 Å (838 cm^{-1}), 1.78 Å (829 cm^{-1}),

201   1.79 Å (822 cm^{-1}), 1.80 Å (809 cm^{-1}), and 1.81 Å (800 cm^{-1}). These values are

202   in accordance with U–O_{yl} bond lengths refined from the X-ray data (1.76-1.79

203   Å) and correlate well with those determined by Weller et al. (2000) (1.74-1.82

204   Å) and Klingensmith et al. (2007) (1.65-1.82 Å) for natural and synthetic Na-

205   and Np-substituted metaschoepite.

206   A weak band at 745 cm^{-1} is assigned as a libration mode of H_2O

207   groups. The large number of bands observed in the region from 590-300 cm^{-1}

208   are attributed to various ν (U–O/OH) stretches of equatorial oxide and

8

209   hydroxide groups; however, we are only able to provide tentative assignments

210   to specific modes based on those given for uranates by Dothée and Camelot

211   (1982) and Dothée et al. (1982). Bands at 581, 545, 528, 509, 485, 461, 449,

212   438, 413, and 397 cm^{-1} are possibly related to ν_3 (U_3O/U_3OH) elongation, U–

213   O_{eq} bridge bending, or H_2O libration modes. In the spectrum of schoepite,

214   Colmenero et al. (2018) assigned all bands between 557 cm^{-1} and 489 cm^{-1} as

215   H_2O libration modes; however, Kirkegaard et al. (2019) notes that because

216   Raman spectroscopy is insensitive to water, and by using the computationally-

217   predicted inelastic neutron scattering spectrum of synthetic metaschoepite,

218   these authors prefer assignments in this region as various in- and out-of-plane

219   stretching ν U–O/OH_{eq} modes. The two weak bands at 342 cm^{-1} and 311 cm^{-1}

220   in bobfinchite may be due either to γ U_3O/U_3OH out-of-plane bending, ν

221     $U_3(OH_3)$, or U_2O/OH bridge elongation. The band at 249 cm^{-1} is assigned as

222   the ν_2 (δ) $(UO_2)^{2+}$ bending vibration and remaining bands below 200 cm^{-1} arise

223   due to uranyl hydroxide bridge bending or phonon modes.

224
225   **Chemical composition**

226   Chemical analyses ($N = 5$) were performed on a JEOL JXA-8230 electron

227   microprobe using Probe for EPMA software (Table 1). The analytical

228   conditions used were 10 kV accelerating voltage, 5 nA beam current and a

229   beam diameter of 10 μm. Raw X-ray intensities were corrected for matrix

230   effects with a ϕρ(z) algorithm (Pouchou and Pichoir, 1985). Bobfinchite

231   contains major U and Na with trace Pb; wavelength dispersive scans for N

232   indicate that no NH_4 is present. No other elements besides O were present

233   above detection limits. A time-dependent intensity correction was applied to

9

234   Na, and because insufficient material was available for a direct determination

235   of H_2O it has been calculated based upon the structure with O = 40 *apfu*. The

236   empirical formula calculated on the basis of O = 40 *apfu* is

237     $Na_{0.99}Pb_{0.02}U_{7.99}O_{40}H_{31.}$ Written structurally, the empirical formula

238   corresponds to $(Na_{0.99},Pb_{0.02}) [(UO_2)_{7.99}O_3(OH)_{11}] \cdot 10H_2O$. The ideal formula

239   is $Na[(UO_2)_8O_3(OH)_{11}] \cdot 10H_2O$, which requires Na_2O 1.19, UO_3 88.06, H_2O

240   10.75, total 100 wt%.

241

242   **Powder X-ray diffraction**

243   X-ray powder diffraction data were obtained using a Rigaku R-Axis

244   Rapid II curved imaging plate microdiffractometer with monochromatized

245   Mo$K\alpha$ radiation. A Gandolfi-like motion on the φ and ω axes was used to

246   randomize diffraction from the sample. Observed *d*-values and intensities

247   were derived by profile fitting using JADE 2010 software (Materials Data,

248   Inc.). Data (in Å for Mo$K\alpha$) are given in Table S1. Unit-cell parameters

249   refined from the powder data using JADE 2010 with whole pattern fitting in

250   space group *Pbcn* are: a = 14.699(3) Å, b = 14.086(2) Å, c = 16.736(3) Å, V =

251   3465.2(11) Å^3.

252
253   **Single-crystal X-ray diffraction**

254   An optically clean disc-shaped crystal measuring 30 x 20 x 10 µm was

255   chosen for the single-crystal X-ray diffraction experiment. Data were collected

256   at room temperature using monochromatized Mo$K\alpha$ X-rays from a microfocus

257   source and a Photon II CPAD detector mounted to a Bruker D8 Venture three-

258   circle diffractometer. The Apex II software package was used for processing

259   collected diffraction data, including indexing, integration, scaling and

10

260   corrections for background, polarization and Lorentz effects. A multi-scan

261   semi-empirical absorption correction was made using SADABS (Krause et al.,

262   2015) and an initial model in the space group *Pbcn* was found by the intrinsic-

263   phasing method using SHELXT (Sheldrick, 2015b). The initial model

264   included nearly all atom positions except several O atoms of disordered H_2O

265   groups and the Na2A/Na2B sites. SHELXL-2016 (Sheldrick, 2015a) was used

266   for the refinement of the structure. All atoms except for the Na sites were

267   refined with anisotropic displacement parameters and several H atoms of

268   hydroxyl groups were located. The H atoms were refined with soft restraints

269   on the O–H distance and the U_{iso} of each atom was set to 1.4 times that of the

270   donor O atom. The initial refinements contained relatively strong electron

271   density residuals surrounding U and O atoms (~4-5 $e^-/\text{Å}^3$) which may have

272   originated from the relatively high mosaicity of the tested crystal (0.33º). A

273   culling of weak reflections <0.7 Å significantly reduced the residual ripple

274   density surrounding most atoms (to ~3.5 $e^-/\text{Å}^3$) and improved R_1 and wR

275   values by ~1% and ~3%, respectively. Additional data collection and

276   refinement details are given in Table 3, atom coordinates, equivalent isotropic

277   displacement parameters, and anisotropic displacement parameters are given

278   in Table S1, selected bond distances are listed in Table 4, and a bond valence

279   analysis is provided in Table 5.

280

281   **Features of the Crystal Structure**

282   The structure of bobfinchite contains four unique U sites that each

283   adopt [7]-fold pentagonal bipyramidal coordination (Fig. 4), where the apices

284   of each polyhedron are formed by uranyl oxygen atoms (O_{yl}) multiply bonded

11

285   to the U cation, constituting the approximately linear uranyl cation $(UO_2)^{2+}$

286   (Burns et al., 1997). Each uranyl cation is coordinated five-fold equatorially

287   by O or OH forming pentagonal-bipyramidal polyhedra with linkages that

288   mimic the fourmarierite anion sheet topology (Burns, 2005; Li and Burns,

289   2000; Lussier et al., 2016). The uranyl-oxide-hydroxide sheets in schoepite,

290   metaschoepite, leesite, and kroupaite also adopt the fourmarierite anion

291   topology, which contains edge-sharing pentagons and triangles as its building

292   blocks. The center of each pentagon is populated by a U atom and the

293   triangles, arranged in alternating bow-tie pairs, are vacant.

294

295   **Interlayer arrangement**

296   The interlayer is populated with Na^+ cations and several H_2O groups.

297   Disordered pairs of Na^+ (Na1a, Na1b) cations coordinate with O_{yl} atoms of the

298   sheets. Coordination about the two independent Na^+ sites takes an irregular

299   shape as [7]-fold (Na1A) or [8]-fold (Na1B) polyhedra, where each Na^+ binds

300   to 4 O_{yl} atoms and three O of H_2O groups. Site-scattering refinement reveals

301   that both Na positions are only partially occupied: Na1A 0.45(6), and Na1B

302   0.31(4) with 2× multiplicity, for a combined occupancy of 1.07 Na *afpu* – in

303   close agreement with the average empirical chemistry of 0.99 Na *apfu*.

304   Eight O sites are present in the interlayer corresponding to H_2O molecules that

305   were identified on the basis of incident bond valence sums. Atoms Ow1,

306   Ow3A, Ow3B, and Ow4 form bonds with both Na1A and Na1B cations, with

307   occupancy considerations. Atoms Ow3A and Ow3B are partially occupied at

308   50%. Atoms Ow2, Ow5, Ow6A, and Ow6B do not form bonds to any cations,

309   but accept or donate hydrogen bonds amongst themselves, the other H_2O

310   groups, O_{yl} atoms, and OH groups.

311

Structural Description of the Sheets

313   Minerals of the schoepite family contain variably charged sheets, each

314   having a unique distribution of oxide and hydroxide bridges that satisfy the

315   bonding requirements of the interlayer (Burns, 2005; Lussier et al., 2016;

316   Miller et al., 1996; Plášil, 2018b). We were able to localize H atoms of 4 OH

317   groups except for atom OH12. Bond-valence calculations indicate the OH10,

318   OH12, OH13, OH14, and OH15 sites are fully occupied by OH, whereas atom

319   O11 adopts partial O/OH character and is primarily responsible for balancing

320   sheet charge (Table 5). Ideally, the O11 site contains a 1:1 ratio of OH^- and

321   O^{2-}, for a total of 11 OH^- groups per formula unit. Therefore, based on the

322   calculated bond-valence sums and site scattering refinement, the structural

323   formula of bobfinchite is $Na_{1.07}[(UO_2)_8O_3(OH)_{11}] \cdot 10.04H_2O$.

324

Relation to synthetic phases

326   Bobfinchite belongs to the schoepite family of minerals, whose structures

327   contain identical sheet topologies based on the fourmarierite anion topology.

328   Minerals with structural units built from the fourmarierite anion topology have

329   adaptable sheet charge and distinct distributions of O^{2-} and OH^- dictated by the

330   interlayer content and cation type (Fig. 5). The crystallographic parameters of

331   schoepite family minerals are compared in Table 6. The structure of

332   bobfinchite is most closely related to that of metaschoepite, and though it

333   shares many similarities with those of leesite (Olds et al., 2018) and kroupaite

13

334   (Plášil et al., 2020), these structures crystallize with *Pbca* symmetry, have

335   unique hydroxyl group arrangements and more negatively charged sheets that

336   accommodate higher interlayer Me^+/Me^{2+} content.

337   From a specimen labelled "Paraschoepite – schoep type material,

338   Katanga, Congo," Klingensmith et al. (2007) investigated a crystal of Na-

339   bearing metaschoepite that provided a structural formula somewhat close to

340   bobfinchite, $Na_{0.48}U_8O_{37.91}$. The distribution of hydroxyl groups and

341   arrangement of interlayer Na and H_2O groups in this phase is essentially

342   identical to that of bobfinchite (Fig. 6). Furthermore, the other synthetic Na-

343   and ppm-level Np-doped samples prepared by these authors contain closely

344   overlapping U:Na stoichiometry, and an identical arrangement of hydroxyl

345   groups and interlayer Na and H_2O groups to that found in bobfinchite.

346   Sejkora et al. (2013) encountered "Na-metaschoepite" as pale

347   yellowish orange powder and fine crystalline aggregates up to 3 mm in

348   association with compreignacite, fourmarierite and gypsum in samples from

349   the Jan Evangelista vein, Svornost mine, Jáchymov ore district, Czech

350   Republic. The mineral is orthorhombic, space group *Pbcn*, and the unit-cell

351   parameters refined from X-ray powder diffraction data are: a = 14.025(2), b =

352   16.469(3), c = 14.623(2) Å, and V = 3378(2) Å^3; its chemical analyses

353   correspond to the empirical formula

354    $Na_{0.3}Cu_{0.13}Al_{0.13}K_{0.08}Pb_{0.07}Ca_{0.06}Mg_{0.06}Mn_{0.02}Zn_{0.02}Fe_{0.02}Ni_{0.01}Co_{0.01})_{\Sigma 0.91}[(UO_2$

355    $)_4O_2(SiO_4)_{0.26}(SO_4)_{0.02}(OH)_{4.46}]\cdot 5H_2O$ on the basis of 4 U *apfu*. In Figure 7, we

356   compare chemical data for this phase and related schoepite family minerals.

357

358   **Relation to synthetic phases**

14

359   Based on our observations of the minerals leesite,

360     $K(H_2O)_2[(UO_2)_4O_2(OH)_5]\cdot3H_2O$, and kroupaite,

361     $KPb_{0.5}[(UO_2)_8O_4(OH)_{10}]\cdot10H_2O$, it is possible that a unique Na-rich phase

362   may exist with the ideal composition $Na[(UO_2)_4O_2(OH)_5]\cdot5H_2O$. Though

363   mostly speculative at this time, we wish to provide some guidance on how that

364   phase may be distinguished from bobfinchite, if encountered. As in leesite and

365   kroupaite, this hypothetical phase may adopt *Pbca* symmetry and its interlayer

366   would contain an additional Na site that will coordinate to nearby uranyl O

367   atoms. One can envision the hypothetical location of this additional site and its

368   effect on the topology of the bobfinchite interlayer. There, two of the positions

369   we find most suitable for substitution involve hydrogen bonds formed between

370   O_{yl} atoms O2 and O5 with Ow2 and Ow5. Either H_2O group could feasibly

371   accommodate an additional Na site and their replacement would satisfy local

372   bond-valence requirements of the sheet. Voronoi-Dirichlet polyhedra (VDP)

373   calculations (Blatov, 2004) for leesite and kroupaite reveal that, as expected,

374   their interlayer K and Pb cations fill sites that are best suited to their

375   polyhedral volume (Plášil, 2018b; Plášil et al., 2020; Schindler and

376   Hawthorne, 2004). The large Pb^{2+} cations in kroupaite act as strong Lewis

377   acids and provide significant bond valence to the sheet, offsetting the lower

378   *Me*:H_2O content with respect to leesite (Schindler and Hawthorne, 2004). As it

379   is relatively small (~10 $Å^3$) and forms bonds of similar strength to a hydrogen

380   bond (~0.2 vu), an additional Na^+ cation could feasibly substitute at several

381   different sites in the bobfinchite interlayer without creating significant

382   disruption in the hydrogen bonding network. In order to maintain charge

383   balance it is likely that the bridging oxygen atom O11, or a nearby hydroxyl

15

384   group positioned near the new Na site will exhibit distinct oxide character,

385   with bond valence sums possibly exceeding ~1.8 v.u. Klingensmith et al.

386   (2007) recognized that a linear relationship exists between the bond-valence

387   sum incident on O11 and the b cell parameter for synthetic and natural Na-

388   substituted metaschoepite. The authors suggest that higher OH$^-$ content at O11

389   induces stronger hydrogen bonds, leading to distortion of the UOH sheets and

390   contraction of the b dimension to satisfy bonding requirements with the

391   interlayer. The calculated bond-valence sum for the O11 site in bobfinchite

392   fits their observed trend well, with variable O and OH content accounting for

393   the incorporation of Na (Fig. 8). Thus, introduction of an additional Na site

394   into the hypothetical Na-rich phase will result in an overall larger O^{2-}:$(OH)^-$

395   content, a reduction in hydrogen-bonding interactions with the sheets,

396   manifesting as an expanded b cell dimension with respect to bobfinchite

397   (>14.05 Å). Such is apparently the case for the Na-bearing metaschoepite

398   phase with complex chemical makeup investigated by Sejkora et al. (2013);

399   however, as the material tested was a finely crystalline powder, more detailed

400   crystallographic studies are needed to understand its structural relationship to

401   bobfinchite.

402

403   **Environmental Implications**

404   Most groundwaters, and of course, seawater and brines, contain high

405   concentrations of Na$^+$ that may lead to the formation of bobfinchite when

406   contacting U-bearing materials undergoing oxic corrosion. Since ~2014, we

407   have identified and described more than 20 sodium-bearing uranium minerals,

408   mostly sulfates, that have resulted from the solubilization of U from asphaltic

16

409 materials. These are very important naturalistic observations, as some have

410 proposed to use asphalt and bitumen as a containment barrier and solid waste

411 form for long-term storage of nuclear waste due to their plasticity and ability

412 to bind actinides (Fitzgerald et al., 1970; Schlepp et al., 2001).

413 Surprisingly, we have found no mention of the formation of Na-rich

414 metaschoepite in the publicly available used nuclear fuel alteration literature;

415 though, Na-rich compreignacite and natroboltwoodite are noted alteration

416 products (Finch et al., 1999; Li and Burns, 2001; Wronkiewicz et al., 1992;

417 Wronkiewicz et al., 1996), and given similar PXRD fingerprint and chemistry

418 between compreignacite and bobfinchite, it could have been overlooked or

419 misidentified. As noted by Finch et al. (1997), despite their simple

420 composition, making accurate identification of UOH phases can be

421 exceptionally difficult; the minerals commonly occur as inseparable mixtures

422 and as "massive" polycrystalline aggregates. Most phases in the schoepite

423 family bear strong similarities with one another in unit-cell dimensions and

424 PXRD patterns. In many instances throughout the nuclear waste alteration

425 literature, identifications are designated simply as "schoepite-like, or

426 "clarkeite-like" solids. For example, lysimeter alteration studies made on

427 synthesized metaschoepite in the presence of Na^+ caused complete

428 transformation of the material into a hydrated "clarkeite-like" sodium uranyl

429 oxide with a distinctly different PXRD and Raman spectrum than

430 metaschoepite (Giammar and Hering, 2004). Additionally, synthetic

431 bobfinchite is a likely minor byproduct present in sodium diuranate (SDU)

432 yellow cake obtained during precipitation with sodium hydroxide, or during

433 processing of other uranium oxides (Gayer and Leider, 1955; Schwerdt et al.,

17

434   2019). While many competing mechanisms work to control the migration,

435   precipitation, and speciation of UOH minerals formed in natural and

436   technogenic U-rich systems, the description of bobfinchite provides an

437   essential foundation for defining crucial crystal-chemical and structure-

438   property relationships in the schoepite family.

439
440   **Acknowledgements**

18

450 **References**
451 Bartlett, J.R., and Cooney, R.P. (1989) On the determination of uranium-
452   oxygen bond lengths in dioxouranium(VI) compounds by Raman
453   spectroscopy. Journal of Molecular Structure, 193, 295-300.
454 Benjamin, S.E., LaVerne, J.A., Sigmon, G.E., and Burns, P.C. (2022)
455   Ozone-Facilitated Formation of Uranyl Peroxide in Humid
456   Conditions. Inorganic Chemistry, 61, 20977-20985.
457 Blatov, V.A. (2004) Voronoi–dirichlet polyhedra in crystal chemistry: theory
458   and applications. Crystallography Reviews, 10, 249-318.
459 Brown, I.D. (2006) The Chemical Bond in Inorganic Chemistry: The Bond
460   Valence Model. Oxford University Press, Oxford.
461 Brugger, J., Meisser, N., Etschmann, B., Ansermet, S., and Pring, A. (2011)
462   Paulscherrerite from the Number 2 Workings, Mount Painter Inlier,
463   Northern Flinders Ranges, South Australia: "Dehydrated schoepite"
464   is a mineral after all. American Mineralogist, 96, 229-240.
465 Burns, P.C. (2005) U^{6+} minerals and inorganic compounds: Insights into an
466   expanded structural hierarchy of crystal structures. The Canadian
467   Mineralogist, 43, 1839-1894.
468 Burns, P.C., Ewing, R.C., and Hawthorne, F.C. (1997) The crystal chemistry
469   of hexavalent uranium; polyhedron geometries, bond-valence
470   parameters, and polymerization of polyhedra. The Canadian
471   Mineralogist, 35, 1551-1570.
472 Carter, W.D., and Gualtieri, J.L. (1965) Geology and uranium-vanadium
473   deposits of the La Sal quadrangle, San Juan County, Utah, and
474   Montrose County, Colorado. Professional Paper.
475 Colmenero, F., Cobos, J., and Timón, V. (2018) Periodic Density Functional
476   Theory Study of the Structure, Raman Spectrum, and Mechanical
477   Properties of Schoepite Mineral. Inorganic Chemistry, 57, 4470-
478   4481.
479 Colmenero, F., Fernández, A.M., Cobos, J., and Timón, V. (2019) Periodic
480   DFT Study of the Thermodynamic Properties and Stability of
481   Schoepite and Metaschoepite Mineral Phases. ACS Earth and Space
482   Chemistry, 3, 17-28.
483 Dothée, D.G., and Camelot, M.M. (1982) Vibrational Spectroscopy of
484   potassium hexauranate hydrate. I. Frequencies assignable to oxygen-
485   atoms motions - hypothesis on the structure of the anionic layer.
486   Bulletin de la Société chimique de France, 97-102.
487 Dothée, D.G., Fahys, B.R., and Camelot, M.M. (1982) Vibrational
488   spectroscopy of potassium hexauranate hydrate. II. Motions of
489   hygrogen atoms - hypothesis on the water-structure in the uranate.
490   Bulletin de la Société chimique de France, 103-108.
491 Fallon, C.M., Bower, W.R., Powell, B.A., Livens, F.R., Lyon, I.C., McNulty,
492   A.E., Peruski, K., Mosselmans, J.F.W., Kaplan, D.I., Grolimund, D.,
493   Warnicke, P., Ferreira-Sanchez, D., Kauppi, M.S., Vettese, G.F.,
494   Shaw, S., Morris, K., and Law, G.T.W. (2023) Vadose-zone
495   alteration of metaschoepite and ceramic UO_2 in Savannah River Site
496   field lysimeters. Science of The Total Environment, 862, 160862.
497 Finch, R.J., Buck, E.C., Finn, P.A., and Bates, J.K. (1999) Oxidative
498   Corrosion of Spent UO_2 Fuel in Vapor and Dripping Groundwater at
499   90°C. MRS Online Proceedings Library (OPL), 556, 431.

500 Finch, R.J., Cooper, M.A., Hawthorne, F.C., and Ewing, R.C. (1996) The
501   crystal structure of schoepite, $[(UO_2)_8O_2(OH)_{12}](H_2O)_{12}$. The
502   Canadian Mineralogist, 34, 1071-1088.
503 Finch, R.J., and Ewing, R.C. (1992) The corrosion of uraninite under
504   oxidizing conditions. Journal of Nuclear Materials, 190, 133-156.
505 Finch, R.J., Hawthorne, F.C., and Ewing, R.C. (1998) Structural relations
506   among schoepite, metaschoepite and "dehydrated schoepite". The
507   Canadian Mineralogist, 36, 831-845.
508 Finch, R.J., Hawthorne, F.C., Miller, M.L., and Ewing, R.C. (1997)
509   Distinguishing among schoepite, $[(UO_2)_8O_2(OH)_{12}](H_2O)_{12}$, and
510   related minerals by X-ray powder diffraction. Powder Diffraction, 12,
511   230-238.
512 Finch, R.J., Miller, M.L., and Ewing, R.C. (1992) Weathering of natural
513   uranyl oxide hydrates - schoepite polytypes and dehydration effects.
514   Radiochimica Acta, 58-9, 433-443.
515 Finch, R.J., and Murakami, T. (1999) Systematics and paragenesis of
516   uranium minerals. In P.C. Burns, and R.J. Finch, Eds. Uranium:
517   Mineralogy, Geochemistry and the Environment, 38, p. 91-179.
518   Mineralogical Society of America.
519 Fitzgerald, C.L., Godbee, H.W., Blanco, R.E., and Davis, W. (1970) The
520   Feasibility of Incorporating Radioactive Wastes in Asphalt or
521   Polyethylene. Nuclear Applications and Technology, 9, 821-829.
522 Frost, R.L., Čejka, J., and Weier, M.L. (2007) Raman spectroscopic study of
523   the uranyl oxyhydroxide hydrates: becquerelite, billietite, curite,
524   schoepite and vandendriesscheite. Journal of Raman Spectroscopy,
525   38, 460-466.
526 Gayer, K.H., and Leider, H. (1955) The Solubility of Uranium Trioxide,
527      $UO_3 \cdot H_2O$, in Solutions of Sodium Hydroxide and Perchloric Acid at
528   25°1. Journal of the American Chemical Society, 77, 1448-1450.
529 Giammar, D.E., and Hering, J.G. (2004) Influence of Dissolved Sodium and
530   Cesium on Uranyl Oxide Hydrate Solubility. Environmental Science
531   & Technology, 38, 171-179.
532 Gorman-Lewis, D., Burns, P.C., and Fein, J.B. (2008) Review of uranyl
533   mineral solubility measurements. Journal of Chemical
534   Thermodynamics, 40, 335-352.
535 Hanson, B., McNamara, B., Buck, E., Friese, J., Jenson, E., Krupka, K., and
536   Arey, B. (2005) Corrosion of commercial spent nuclear fuel. 1.
537   Formation of studtite and metastudtite. Radiochimica Acta, 93, 159-
538   168.
539 Kirkegaard, M.C., Niedziela, J.L., Miskowiec, A., Shields, A.E., and
540   Anderson, B.B. (2019) Elucidation of the Structure and Vibrational
541   Spectroscopy of Synthetic Metaschoepite and Its Dehydration
542   Product. Inorganic Chemistry, 58, 7310-7323.
543 Klingensmith, A.L., Deely, K.M., Kinman, W.S., Kelly, V., and Burns, P.C.
544   (2007) Neptunium incorporation in sodium-substituted
545   metaschoepite. American Mineralogist, 92, 662-669.
546 Knope, K.E., and Soderholm, L. (2013) Solution and Solid-State Structural
547   Chemistry of Actinide Hydrates and Their Hydrolysis and
548   Condensation Products. Chemical Reviews, 113, 944-994.
549 Krause, L., Herbst-Irmer, R., Sheldrick, G.M., and Stalke, D. (2015)
550   Comparison of silver and molybdenum microfocus X-ray sources for

20

551   single-crystal structure determination. Journal of Applied
552   Crystallography, 48, 3-10.
553 Li, Y., and Burns, P.C. (2000) Investigations of crystal-chemical variability
554   in lead uranyl oxide hydrates. II. Fourmarierite. The Canadian
555   Mineralogist, 38, 737-749.
556 -. (2001) The structures of two sodium uranyl compounds relevant to nuclear
557   waste disposal. Journal of Nuclear Materials, 299, 219-226.
558 Lussier, A.J., Burns, P.C., and King-Lopez, R. (2016) A revised and
559   expanded structure hierarchy of natural and synthetic hexavalent
560   uranium compounds. The Canadian Mineralogist, 54, 177-283.
561 Mandarino, J.A. (2007) The Gladstone-Dale compatibility of minerals and
562   its use in selecting mineral species for further study. The Canadian
563   Mineralogist, 45, 1307-1324.
564 Miller, M.L., Finch, R.J., Burns, P.C., and Ewing, R.C. (1996) Description
565   and classification of uranium oxide hydrate sheet anion topologies.
566   Journal of Materials Research, 11, 3048-3056.
567 Olds, T.A., Plášil, J., Kampf, A.R., Spano, T., Haynes, P., Carlson, S.M.,
568   Burns, P.C., Simonetti, A., and Mills, O.P. (2018) Leesite,
569    $K(H_2O)_2[(UO_2)_4O_2(OH)_5] \cdot 3H_2O$, a new K-bearing schoepite-family
570   mineral from the Jomac mine, San Juan County, Utah, U.S.A.
571   American Mineralogist, 103, 143-150.
572 Plášil, J. (2014) Oxidation-hydration weathering of uraninite: the current
573   state-of-knowledge. Journal of Geosciences, 59, 99-114.
574 Plášil, J. (2018a) The crystal structure of uranyl-oxide mineral schoepite,
575    $[(UO_2)_4O(OH)_6](H_2O)_6$, revisited. Journal of Geosciences, 63, 65-73.
576 -. (2018b) Uranyl-oxide hydroxy-hydrate minerals: their structural
577   complexity and evolution trends. European Journal of Mineralogy,
578   30, 237-251.
579 Plášil, J., Kampf, A.R., Olds, T.A., Sejkora, J., Škoda, R., Burns, P.C., and
580   Čejka, J. (2020) The new K, Pb-bearing uranyl-oxide mineral
581   kroupaite: Crystal-chemical implications for the structures of uranyl-
582   oxide hydroxy-hydrates. American Mineralogist, 105, 561-568.
583 Pouchou, J.L., and Pichoir, F. (1985) "PAP" (φρZ) procedure for improved
584   quantitative microanalysis. In J.T. Armstrong, Ed. Microbeam
585   Analysis, p. 104-106. San Francisco Press, California.
586 Riba, O., Walker, C., and Ragnarsdottir, K.V. (2005) Kinetic Studies of
587   Synthetic Metaschoepite under Acidic Conditions in Batch and Flow
588   Experiments. Environmental Science & Technology, 39, 7915-7920.
589 Schindler, M., and Hawthorne, F.C. (2004) A bond-valence approach to the
590   uranyl-oxide hydroxy-hydrate minerals: Chemical composition and
591   occurrence. The Canadian Mineralogist, 42, 1601-1627.
592 Schlepp, L., Elie, M., Landais, P., and Romero, M.A. (2001) Pyrolysis of
593   asphalt in the presence and absence of water. Fuel Processing
594   Technology, 74, 107-123.
595 Schoep, A., and Stradiot, S. (1947) Paraschoepite and epiianthinite, two new
596   uranium minerals from Shinkolobwe (Belgian Congo). American
597   Mineralogist, 32, 344-350.
598 Schwerdt, I.J., Hawkins, C.G., Taylor, B., Brenkmann, A., Martinson, S.,
599   and McDonald Iv, L.W. (2019) Uranium oxide synthetic pathway
600   discernment through thermal decomposition and morphological
601   analysis. 107, 193-205.

21

602 Sejkora, J., Plášil, J., and Bureš, B. (2013) Unusual assocation of supergene
603   uranium minerals from the Jan Evangelista vein, Jáchymov (Czech
604   Republic). Bulletin mineralogicko-petrologického oddělení
605   Národního Muzea (Praha), 21, 143-156.
606 Shawe, D.R. (2011) Uranium-Vanadium Deposits of the Slick Rock District,
607   Colorado. 80 p, Reston, Virginia.
608 Sheldrick, G.M. (2015a) Crystal structure refinement with SHELXL. Acta
609   Crystallographica Section C-Crystal Structure Communications, 71,
610   3-8.
611 Sheldrick, G.M. (2015b) SHELXT - Integrated space-group and crystal-
612   structure determination. Acta Crystallographica Section A, 71, 3-8.
613 Sowder, A.G., Clark, S.B., and Field, R.A. (1999) The transformation of
614   uranyl oxide hydrates: The effect of dehydration on synthetic
615   metaschoepite and its alteration to becquerelite. Environmental
616   Science & Technology, 33, 3552-3557.
617 Sunder, S., Shoesmith, D.W., Christensen, H., and Miller, N.H. (1992)
618   Oxidation of UO_2 fuel by the products of gamma radiolysis of water.
619   Journal of Nuclear Materials, 190, 78-86.
620 Taylor, J.C., and Hurst, H.J. (1971) The hydrogen-atom locations in the
621   [alpha] and [beta] forms of uranyl hydroxide. Acta Crystallographica
622   Section B, 27, 2018-2022.
623 Taylor, P., Wood, D.D., Owen, D.G., and Park, G.-I. (1991) Crystallization
624   of U_3O_8 and hydrated UO_3 on UO_2 fuel in aerated water near 200°C.
625   Journal of Nuclear Materials, 183, 105-114.
626 Walenta, K., and Theye, T. (2012) Heisenbergite, a new uranium mineral
627   from the uranium deposit of Menzenschwand in the Southern Black
628   Forest, Germany. Neues Jahrbuch für Mineralogie, 189, 117-123.
629 Weller, M.T., Light, M.E., and Gelbrich, T. (2000) Structure of uranium(VI)
630   oxide dihydrate, $UO_3 \cdot 2H_2O$; synthetic meta-schoepite
631     $(UO_2)_4O(OH)_6 \cdot 5H_2O$. Acta Crystallographica Section B-Structural
632   Science, 56, 577-583.
633 Wronkiewicz, D.J., Bates, J.K., Gerding, T.J., Veleckis, E., and Tani, B.S.
634   (1992) Uranium release and secondary phase formation during
635   unsaturated testing of UO_2 at 90°C. Journal of Nuclear Materials,
636   190, 107-127.
637 Wronkiewicz, D.J., Bates, J.K., Wolf, S.F., and Buck, E.C. (1996) Ten-year
638   results from unsaturated drip tests with UO_2 at 90°C: implications for
639   the corrosion of spent nuclear fuel. Journal of Nuclear Materials, 238,
640   78-95.
641 Zhang, Y., Lu, K.T., and Zheng, R. (2022) Synthetic uranium oxide hydrate
642   materials: Current advances and future perspectives. Dalton
643   Transactions, 51, 2158-2169.
644
645
646
647
648
649
650
651
652

653
654 **FIGURE CAPTIONS**
655
656 Figure 1. Lozenge-shaped crystals of bobfinchite on black asphaltite with
657 bladed natrozippeite and gypsum. Horizontal field of view is 0.5 mm.
658
659 Figure 2. Crystal drawing of bobfinchite, clinographic projection in non-
660 standard orientation.
661
662 Figure 3. The fitted baseline-corrected Raman spectrum of bobfinchite taken
663 with a 785 nm laser from 1800-50 cm^{-1}.
664
665 Figure 4. The crystal structure of bobfinchite viewed down c. The unit cell is
666 indicated by dashed blue lines. Na atoms are presented as magenta spheres,
667 while O and H atoms of H_2O groups are indicated by red and white spheres,
668 respectively.
669
670 Figure 5. A comparison of anion sheet topologies of analogous schoepite
671 family minerals, including OH$^-$ and interlayer cation distributions. Black
672 circles highlight vertices containing OH$^-$ and bare vertices represent O^{2-}. The
673 mixed O/OH atom O11 is represented by a two-toned black and gray sphere
674 in the sheets of bobfinchite and its related synthetic analogues from
675 Klingensmith et al. (2007). Potassium (blue), lead (orange), sodium (yellow).
676
677 Figure 6. A side-by-side comparison of the interlayer atomic arrangement in
678 bobfinchite and the Na-bearing analogues studied by Klingensmith et al.
679 (2007).
680
681 Figure 7. Ternary plot of compositional data for bobfinchite and related
682 phases.
683
684 Figure 8. The linear relationship between incident bond-valence sum at O11
685 and the b unit cell dimension. Refer to Table 6 for sample labels listed by
686 Klingensmith et al. (2007).
687
688
689
690
691
692 Table 1. Chemical composition of bobfinchite.

Constituent	Mean	Range	Stand. Dev.	Standard
Na_2O	1.15	1.01–1.27	0.09	albite
PbO	0.20	0.14–0.26	0.05	PbS
UO_3	85.59	83.81–86.60	1.12	syn. UO_2
H_2O*	10.46	-	-	-
Total	**97.40**			

693 * based on the structure
694

23

695 Table 2. Powder X-ray data (d in Å) for bobfinchite. Only $I \geq 2$ calculated lines are listed.

I_{obs}	d_{obs}	d_{calc}	I_{calc}	hkl
		8.6587	1	1 1 1
		8.3462	1	0 0 2
100	7.3366	7.3125	100	2 0 0
		7.2488	1	1 0 2
		6.4706	2	0 2 1
		6.0452	1	2 1 1
		5.5001	1	2 0 2
3	5.0595	5.0426	2	1 2 2
4	4.8636	4.8766	1	1 1 3
		4.8458	1	2 2 1
6	4.4323	4.4394	4	3 1 1
		4.3294	1	2 2 2
		4.1786	1	1 2 3
		4.0129	1	1 0 4
21	3.6582	3.6562	18	4 0 0
		3.6101	1	3 2 2
50	3.5901	3.5871	36	0 2 4
		3.5477	3	3 1 3
22	3.5164	3.5097	16	0 4 0
		3.4838	1	1 2 4
		3.4613	1	4 1 1
		3.3759	1	3 3 0
		3.3437	2	1 4 1
		3.3089	1	3 3 1
63	3.2288	3.2205	50	2 2 4
		3.1702	1	3 0 4
36	3.1756	3.1641	24	2 4 0
		2.9685	1	0 4 3
		2.8862	1	3 3 3
		2.8223	2	5 1 1
		2.8077	1	3 4 1
		2.7821	1	0 0 6
4	2.7642	2.7505	2	2 4 3
		2.7330	1	1 0 6
		2.6418	1	1 4 4
		2.5863	1	0 2 6
		2.5689	1	5 2 2
20	2.5684	2.5605	15	4 2 4
10	2.5403	2.5461	2	5 1 3
		2.5320	7	4 4 0
		2.4707	1	1 5 3
4	2.4445	2.4534	1	5 3 1
		2.4375	3	6 0 0
		2.4163	1	3 0 6
		2.3771	1	6 1 1
3	2.3138	2.3172	1	0 6 1
		2.3026	1	6 2 0
2	2.264	2.2654	1	5 3 3
		2.2579	1	0 2 7
		2.2293	1	3 5 3
4	2.2215	2.2267	1	1 6 2
		2.2089	1	2 6 1
		2.1802	1	0 4 6
5	2.1596	2.1564	3	1 4 6
		2.1338	1	1 6 3
		2.1176	1	3 1 7
		2.1019	1	3 5 4
9	2.0945	2.0893	1	2 4 6
		2.0865	4	0 0 8
		2.0656	1	1 0 8
17	2.0447	2.0509	2	7 1 1
		2.0409	8	0 6 4
		2.0161	9	6 2 4
		2.0108	1	5 5 1
23	2.0134	2.0065	5	2 0 8
		2.0020	4	6 4 0
		1.9902	2	3 4 6
		1.9816	1	1 2 8
20	1.9726	1.9724	1	3 6 3
		1.9658	11	2 6 4
		1.9572	1	4 6 1
5	1.9485	1.9472	2	7 2 2
		1.9372	2	7 1 3
		1.9078	1	7 3 0
5	1.9055	1.9034	1	5 5 3
		1.8998	1	1 6 5
		1.8954	1	7 3 1
4	1.846	1.8519	1	7 1 4
		1.8324	1	5 1 7
		1.8281	2	8 0 0
8	1.8191	1.8222	1	5 5 4
		1.8122	3	4 0 8
		1.8046	1	7 3 3
17	1.791	1.7935	3	0 4 8
		1.7821	6	4 6 4
		1.7802	1	1 4 8
4	1.7651	1.7691	1	8 2 0
		1.7549	2	0 8 0
12	1.745	1.7480	1	5 4 6
		1.7419	5	2 4 8
		1.7329	1	1 8 1
6	1.7115	1.7190	1	5 3 7
		1.7064	3	2 8 0
7	1.6726	1.6745	1	8 0 4
		1.6736	1	0 8 3
		1.6706	1	7 0 6
		1.6593	1	1 6 7
11	1.635	1.6431	1	3 8 1
		1.6314	1	2 8 3
		1.6288	4	8 2 4
		1.6214	2	8 4 0
		1.6140	2	1 2 10
11	1.6147	1.6102	4	4 4 8
		1.6067	1	9 1 1
		1.6049	1	7 5 3
7	1.5863	1.5851	2	6 0 8
		1.5821	2	4 8 0
		1.5800	1	3 6 7
7	1.5626	1.5648	3	6 6 4
		1.5617	1	7 1 7
		1.5554	2	9 2 2
		1.5503	1	9 1 3
5	1.5392	1.5407	2	3 2 10
		1.5286	1	9 3 1
		1.5218	1	4 8 3
4	1.5144	1.5191	1	4 6 7
		1.5113	1	8 4 4
		1.5085	1	7 4 6
		1.4897	1	7 3 7
		1.4798	1	9 3 3
		1.4767	1	1 8 6
		1.4446	2	6 4 8
5	1.4488	1.4317	1	10 2 0
		1.4242	1	6 8 0
4	1.4214	1.4198	2	5 2 10

696	Table 3. Data collection and structure refinement details for bobfinchite.	
697	Diffractometer	Bruker D8 Venture & PHOTON II detector
698	X-ray radiation/power	Mo$K\alpha$ ($\lambda = 0.71073$ Å)/50 kV, 30 mA
699	Temperature	298(2) K
700	Structural Formula	$H_8Na_{1.07}O_{40.04}U_8$
701	Space group	*Pbcn*
702	Unit cell dimensions	$a = 14.6249(9)$ Å
703		$b = 14.0389(10)$ Å
704		$c = 16.6923(10)$Å
705	*V*	3427.2(4) Å^3
706	*Z*	4
707	Density (for above formula)	4.995 g cm^{-3}
708	Absorption coefficient	37.795 mm^{-1}
709	*F*(000)	4304
710	Crystal size	$30 \times 20 \times 10$ µm
711	θ range	2.35 to 30.51°
712	Index ranges	$-20 \leq h \leq 20, -20 \leq k \leq 29, -23 \leq l \leq 23$
713	Reflections collected/unique	75656/5228; $R_{int} = 0.10$
714	Reflections with $I > 4\sigma I$	3770
715	Completeness to $\theta = 30.51°$	100%
716	Refinement method	Full-matrix least-squares on F^2
717	Parameter/restraints	256/4
718	GoF	1.077
719	Final *R* indices [$I > 4\sigma I$]	$R_1 = 0.0330, wR_2 = 0.0660$
720	*R* indices (all data)	$R_1 = 0.0606, wR_2 = 0.0792$
721	Largest diff. peak/hole	+3.46/–2.19 e$^-$ A^{-3}

722 $R_{int} = \Sigma|F_o^2 - F_o^2(\text{mean})|/\Sigma[F_o^2]$. GoF $= S = \{\Sigma[w(F_o^2 - F_c^2)^2]/(n-p)\}^{1/2}$. $R_1 =$
723 $\Sigma||F_o| - |F_c||/\Sigma|F_o|$. $wR_2 = \{\Sigma[w(F_o^2 - F_c^2)^2]/\Sigma[w(F_o^2)^2]\}^{1/2}$; $w =$
724 $1/[\sigma^2(F_o^2) + (aP)^2 + bP]$ where *a* is 0.022, *b* is 47.97 and *P* is
725 $[2F_c^2 + \text{Max}(F_o^2, 0)]/3$.

726
727
728
729
730
731
732
733
734
735
736
737
738
739
740
741
742

Table 4. Selected bond distances (Å) for bobfinchite.

U1		U2		U3	
−O4	1.779(7)	−O3	2.248(7)	−O1	1.787(7)
−O5	1.770(8)	−O6	1.789(7)	−O2	1.756(7)
−OH10	2.429(7)	−O9	1.780(7)	−O3	2.228(7)
−O11	2.278(7)	−O11^{ii}	2.291(7)	−O11^{vii}	2.339(7)
−OH12	2.317(7)	−OH13^{viii}	2.560(6)	−OH10^{viii}	2.454(6)
−OH14	2.422(6)	−OH14^{vii}	2.396(6)	−OH13	2.435(6)
−OH15^{viii}	2.528(6)	−OH15^{vii}	2.469(7)	−OH14^{vii}	2.605(6)
<U−O$_{yl}$>	1.775	<U−O$_{yl}$>	1.785	<U−O$_{yl}$>	1.772
∠O$_{yl}$-U-O$_{yl}$	177.9(3)	∠O$_{yl}$-U-O$_{yl}$	178.3(4)	∠O$_{yl}$-U-O$_{yl}$	176.4(3)
<U−O$_{eq}$>	2.397	<U−O$_{eq}$>	2.393	<U−O$_{eq}$>	2.412

U4		Na1A		Na1B	
−O3	2.215(7)	−O5^{vi}	2.839(11)	−Ow2	2.98(3)^{iii}
−O7	1.783(7)	−O5^{viii}	2.839(11)	−Ow5	2.66(2)^{viii}
−O8	1.784(7)	−O8	2.426(15)	−Ow5	2.99(2)^{vi}
−OH10^{viii}	2.613(7)	−O8^{iii}	2.426(15)	−Ow8	2.55(2)^{iii}
−OH12	2.322(7)	−Ow1	2.30(3)	−Ow8	2.80(2)
−OH13^{viii}	2.452(6)	−Ow3A	2.45(3)	−Ow1	2.15(3)
−OH15	2.416(7)	−Ow3A^{iii}	2.45(3)	−Ow3B	2.64(5)^{iii}
<U−O$_{yl}$>	1.784	<Na1A−O>	2.53	−Ow3A	3.14(4)^{iii}
∠O$_{yl}$-U-O$_{yl}$	177.7(3)			<Na1B−O>	2.74
<U−O$_{eq}$>	2.404				

Hydrogen Bonds

	D-H	H-A	D-A	∠DHA
OH10–H10···Ow6A	0.96(3)	1.90(5)	2.832(8)	163(10)
OH10–H10···Ow6B	0.96(3)	1.98(5)	2.904(16)	160(10)
OH13–H13···Ow5	0.95(3)	1.84(3)	2.784(12)	176(10)
OH14–H14···Ow4^{iii}	0.97(3)	1.87(4)	2.836(13)	172(10)
OH15–H15···Ow2	0.96(3)	1.83(3)	2.785(12)	174(11)

744 Symmetry codes: (ii) -x+1/2, -y+1/2, z+1/2; (iii) -x, y, -z+1/2;
745 (vi) x-1/2, y-1/2, -z-1/2; (vii) x, -y, z-1/2; (viii) -x-1/2, y-1/2, z.
746
747
748
749
750
751
752
753
754
755
756
757
758
759
760
761

Table 5. Bond valence analysis for bobfinchite. Values are expressed in valence units (v.u.).[*]

	U1	U2	U3	U4	Na1A*	Na1B**	H10	H13	H14	H15	Σ_{anion}	O type
O1			1.73								1.73	yl
O2			1.85			0.05					1.89	yl
O3		0.65	0.68	0.70							2.03	O
O4	1.76										1.76	yl
O5	1.80				$0.07^{×2↓→}$	0.10/0.05					1.90	yl
O6		1.72									1.72	yl
O7				1.74							1.74	yl
O8				1.74	$0.18^{×2↓→}$	0.18/0.07					1.96	yl
O9		1.75									1.75	yl
OH10	0.44		0.44	0.30			0.80				1.99	OH
O11	0.61	0.60	0.54								1.75	O/OH
OH12	0.56			0.56							1.12	OH
OH13		0.34	0.44	0.42				0.84			2.04	OH
OH14	0.45	0.48	0.31						0.81		2.05	OH
OH15	0.36	0.41		0.45						0.83	2.05	OH
Ow1					0.24	0.34					0.58	H_2O
Ow2										0.04	0.40	H_2O
Ow3A[†]					$0.16^{×2↓→}$	0.10					0.42	H_2O
Ow3B[†]						0.03					0.03	H_2O
Ow4									0.03		0.03	H_2O
Ow5								0.04			0.04	H_2O
Ow6A[‡]							0.03				0.03	H_2O
Ow6B[§]							0.02				0.02	H_2O
Σ_{cation}	5.99	5.95	5.98	5.92	1.05	0.87	0.85	0.88	0.84	0.87		

[*] Bond valence parameters for U and Na are from Gagné and Hawthorne (2015), and $H^+–O^{2-}$ <1.05 Å from Brown (2006). Anion sums for Na1A/B–O5 and Na1A/B–O8 are scaled to Na occupancy. Refined site occupancy = [*]0.45(6), [**]0.31(4), [†] 0.5, [‡] 0.69(5), [§] 0.35(5).

Table 6. A comparison of the crystallographic parameters of schoepite-family minerals and analogous phases.

Phase	Occurrence	a [Å]	b [Å]	c [Å]	V [Å^3]	S.G.
Neutral sheets						
schoepite[a]	Shaba, DRC	14.337(3)	16.813(5)	14.731	3426	$P2_1ca$
schoepite[b]	Shinkolobwe, DRC	16.7810(5)	14.7044(4)	14.2985(5)	3528	*Pbca*
metaschoepite[c]	synthetic	14.6861(4)	13.9799(3)	16.7063(5)	3439	*Pbcn*
paraschoepite[d]	Shinkolobwe, DRC	14.12	16.83	15.22	3617	*Pbca*
heisenbergite[e]	Menzenschwand, DE	13.10(1)	13.76(1)	14.50(1)	2614	$P2_12_12_1;Pna2_1$
paulscherrerite[f]	Radium Ridge, AU	4.288(2)	10.270(6)	6.885(5)	303	$P2;P2_1;P2_1/m$
α-UO$_2$(OH)$_2$[g]	synthetic	4.242(1)	10.302(1)	6.868(1)	300	*Cmca* or *C2cb*
Charged sheets						
bobfinchite	**Colorado, USA**	**14.625**	**14.039**	**16.692**	**3427**	***Pbcn***
Na-rich metaschoepite[h]	Katanga, Congo	14.6801(16)	14.0287(15)	16.7196(17)	3443	*Pbcn*
Na-rich metaschoepite[ih]	synthetic-CRY	14.7050(6)	14.0565(5)	16.7051(6)	3453	*Pbcn*
Na-rich metaschoepite[h]	synthetic-CRY-Np	14.6401(15)	14.0417(14)	16.7044(17)	3434	*Pbcn*
Na-rich metaschoepite[h]	synthetic-AB1	14.6317(27)	14.0417(25)	16.6977(30)	3424	*Pbcn*
Na-rich metaschoepite[h]	synthetic-AB2	14.6592(9)	14.0358(8)	16.7148(10)	3439	*Pbcn*
Na-rich metaschoepite[i]	Jáchymov, CZ	14.64(2)	14.03(1)	16.69(2)	3426	*Pbcn*
K-rich fourmarierite[i]	Jáchymov, CZ	14.025(2)	16.469(4)	14.623(2)	3378	$Bb2_1m$
K-rich fourmarierite[i]	Jáchymov, CZ	13.442(5)	16.611(6)	14.447(2)	3226	$Bb2_1m$
fourmarierite[j]	Shinkolobwe, DRC	14.010(1)	16.401(1)	14.317(1)	3290	$Bb2_1m$
fourmarierite[j]	synthetic	13.938(2)	16.638(3)	14.672(2)	3402	$Bb2_1m$
kroupaite[k]	Jáchymov, CZ	14.8201(8)	14.0958(8)	16.765(1)	3502	*Pbca*
leesite[l]	Utah, USA	14.866(7)	14.126(7)	16.772(8)	3522	*Pbca*

[a] Finch et al. (1996),[b] Plášil (2018a),[c] Weller et al. (2000),[d] Schoep and Stradiot (1947),[e] Walenta and Theye (2012),[f] Brugger et al. (2011),[g] Taylor and Hurst (1971),[h] Klingensmith et al. (2007),[i] Sejkora et al. (2013),[j] Li and Burns (2000),[k] Plášil et al. (2020),[l] Olds et al. (2018).

Figure 1

011

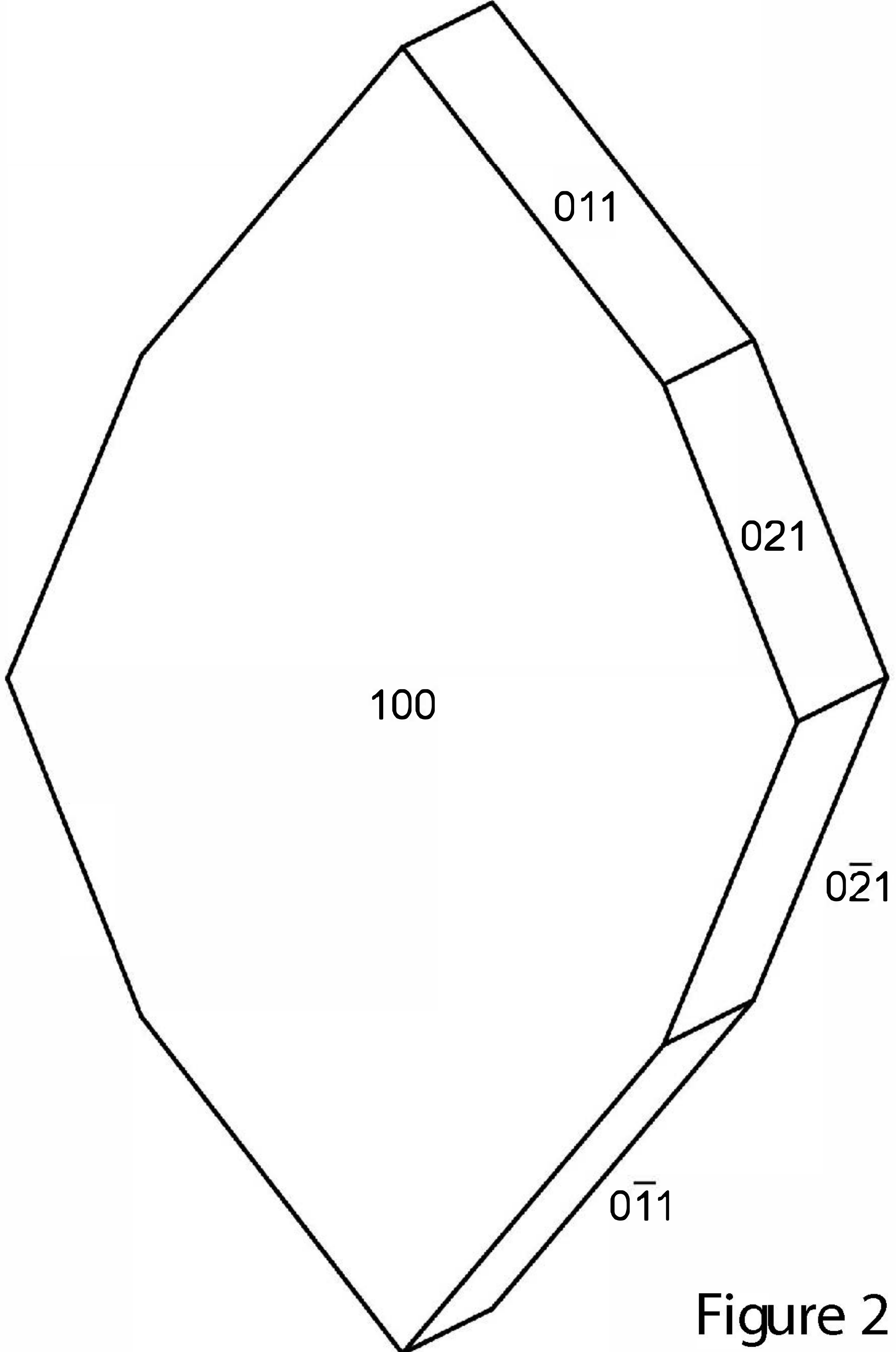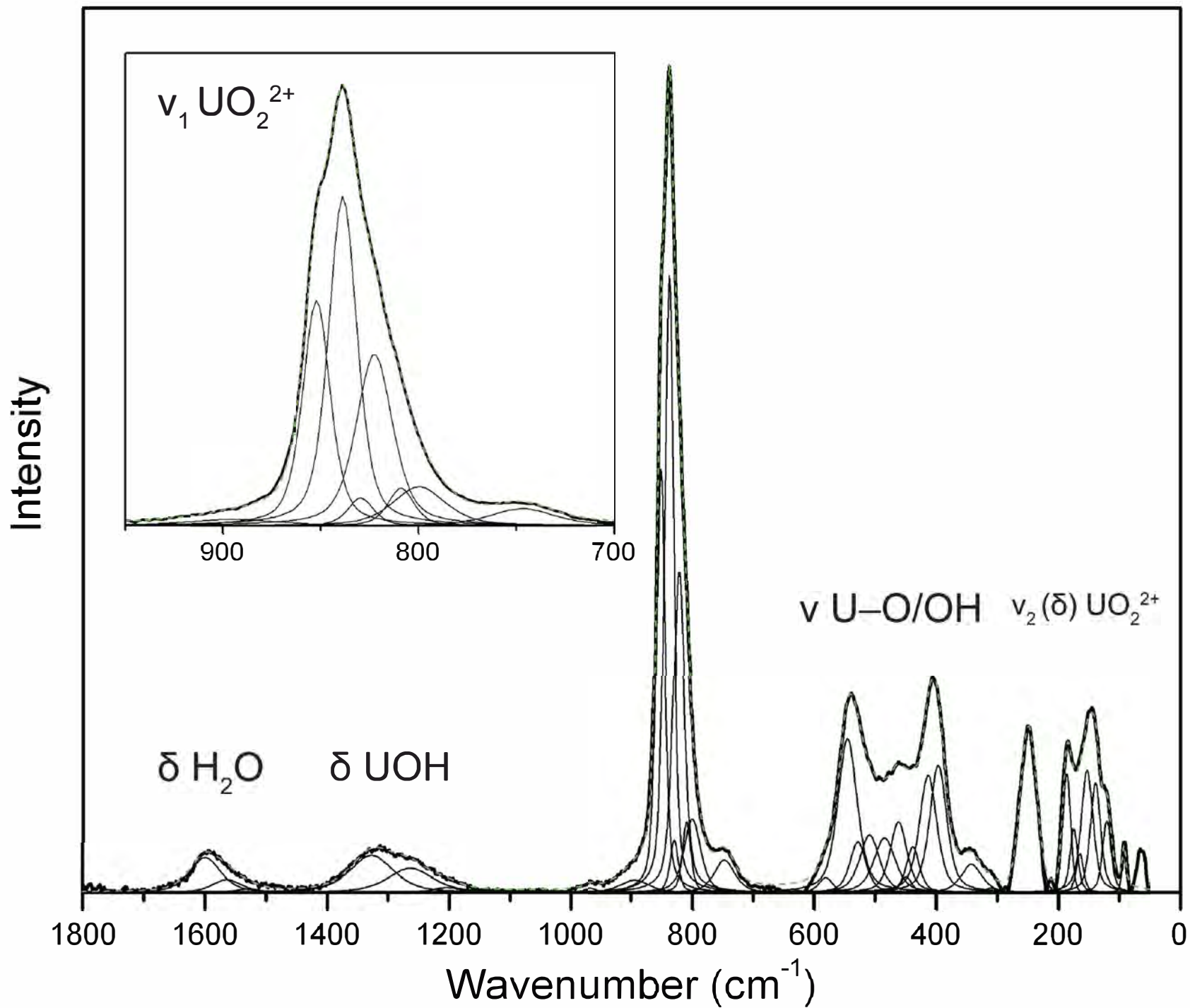021

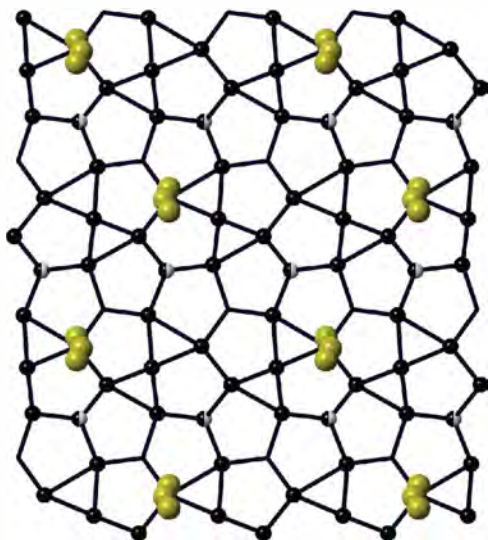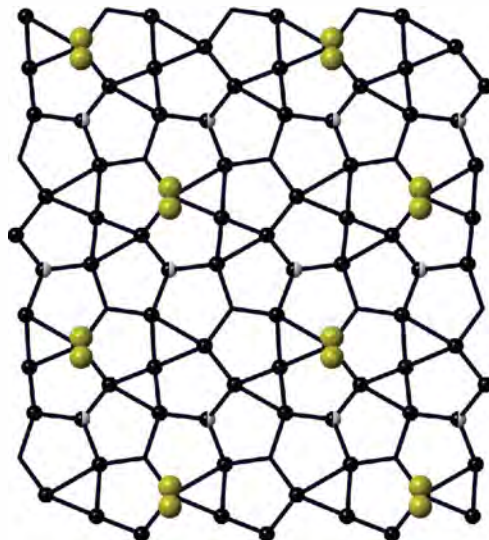100

0$\bar{2}$1

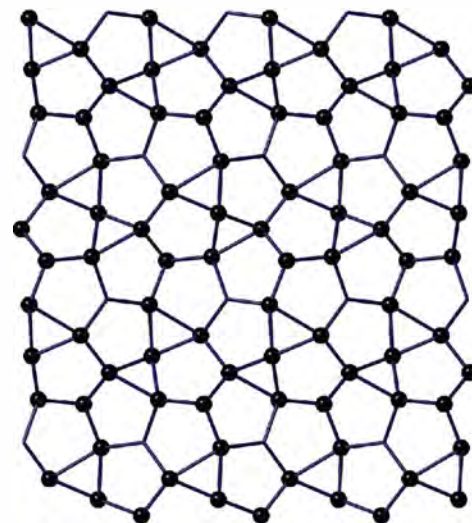0$\bar{1}$1
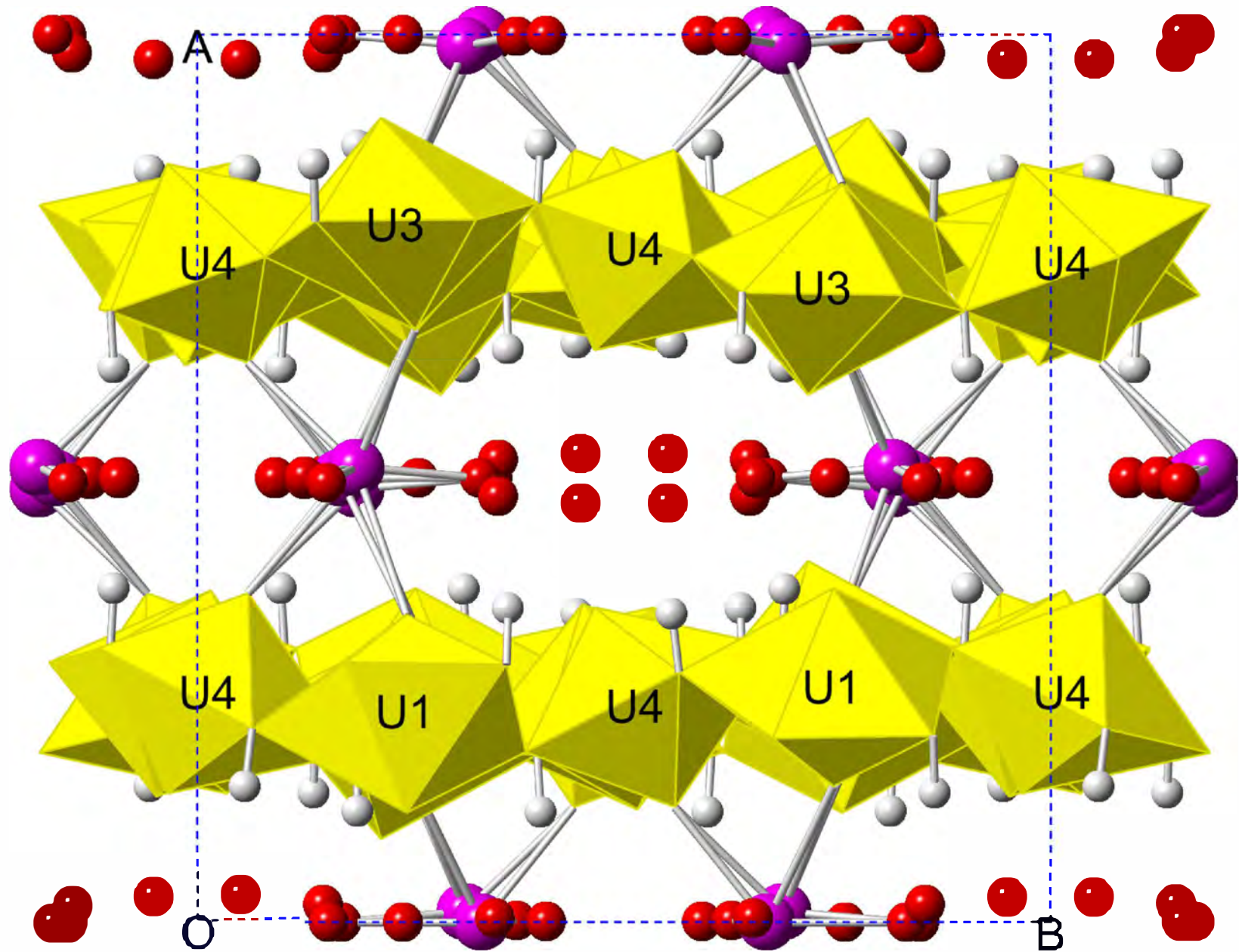
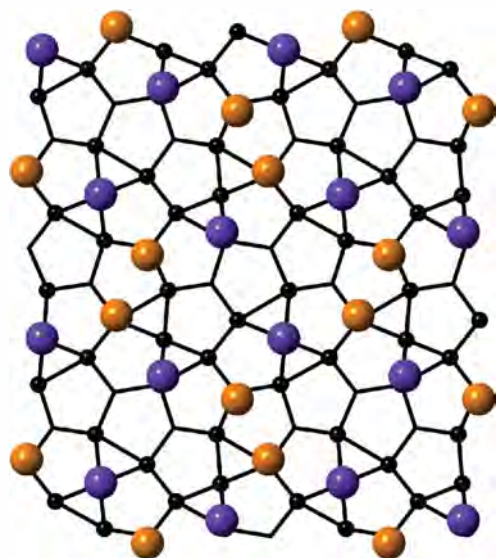Figure 2
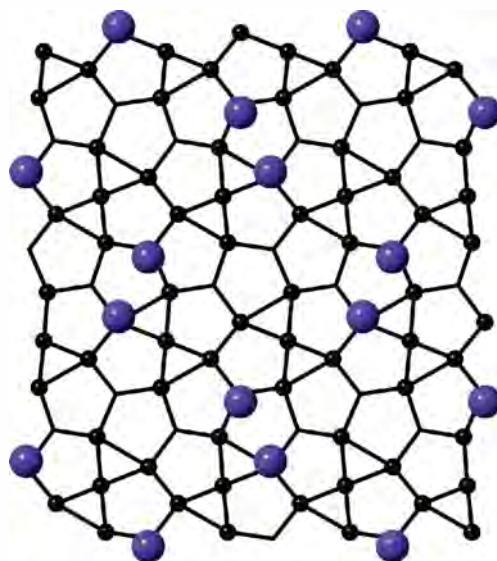
Figure 3

Figure 4

bobfinchite

synthetic analog of bobfinchite

schoepite & metaschoepite

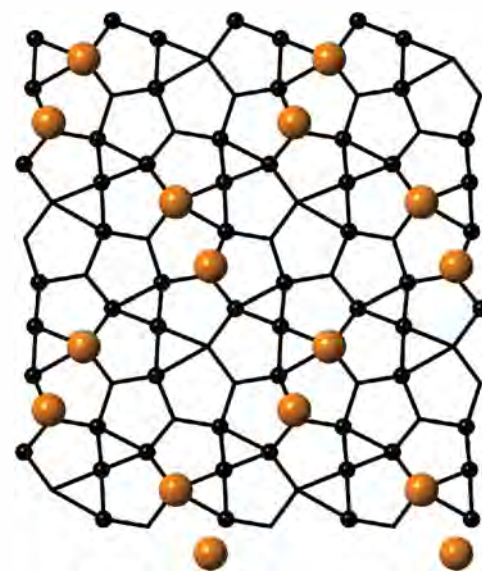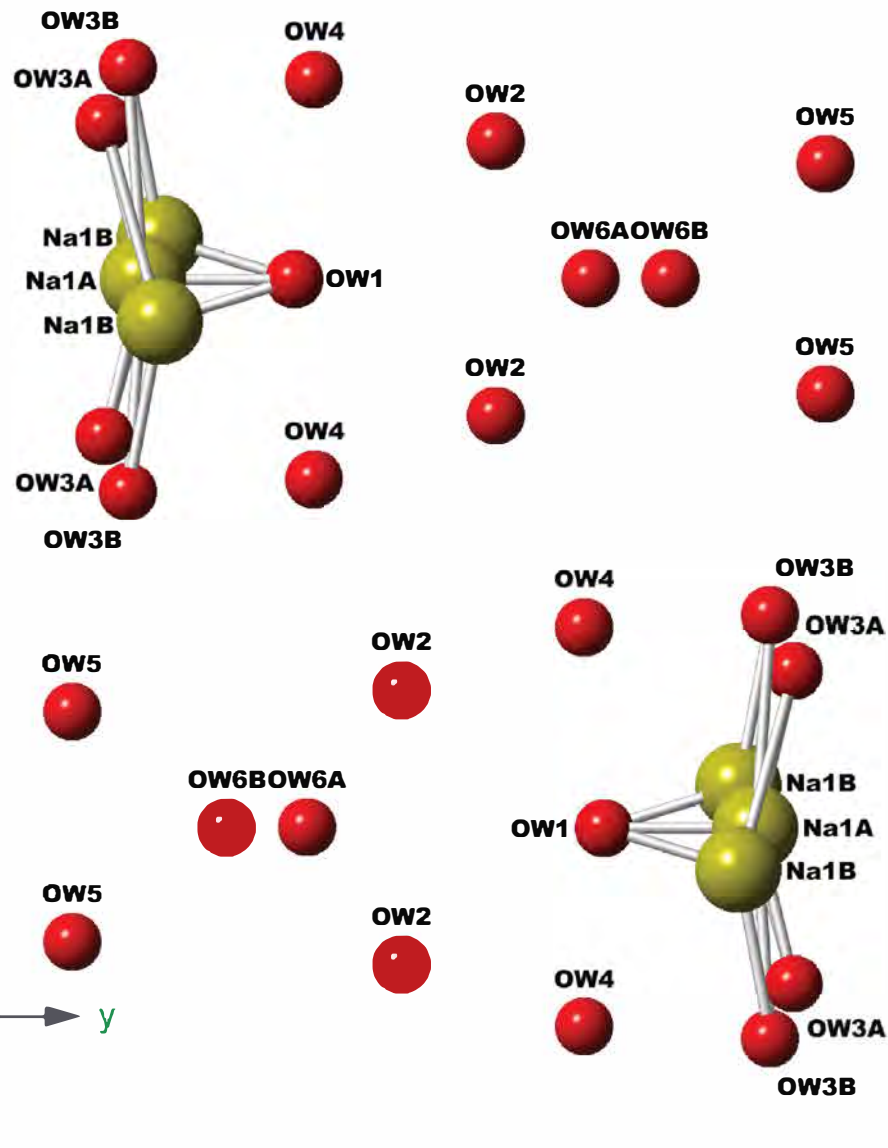**kroupaite**

leesite

fourmarierite

Figure 5

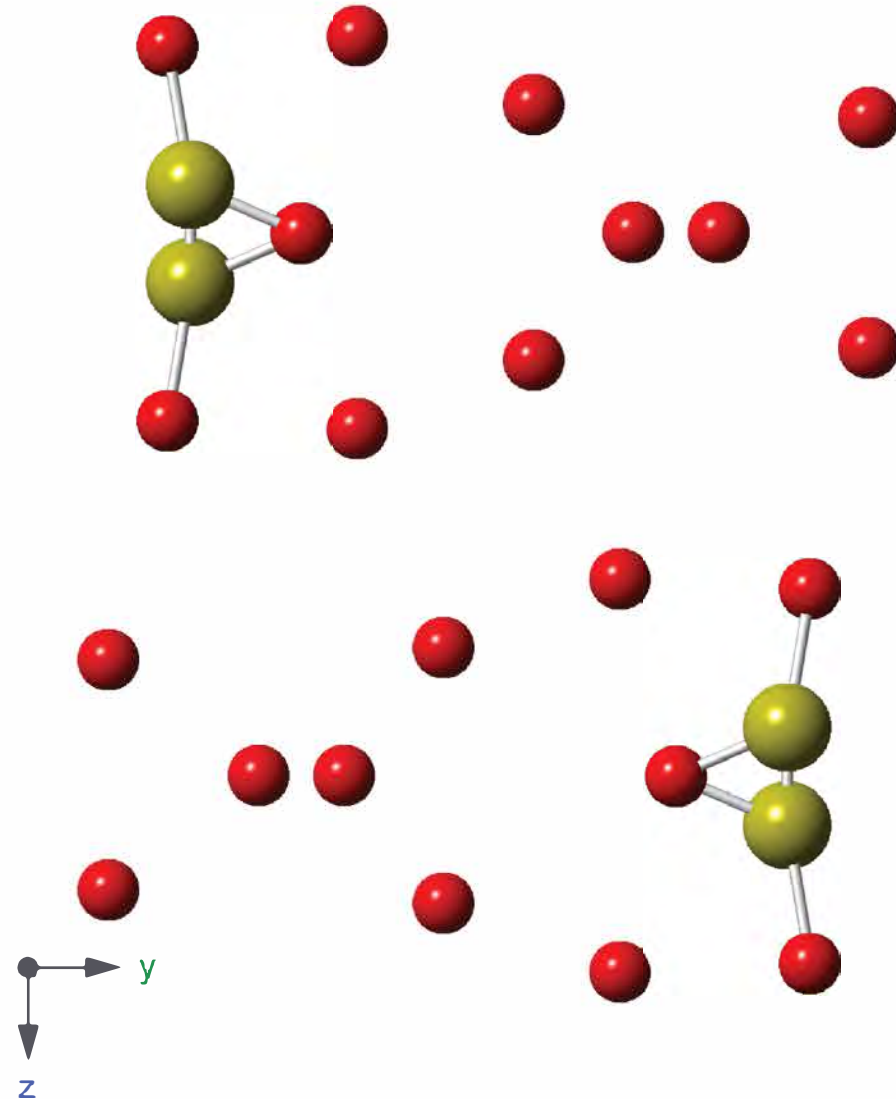**bobfinchite**
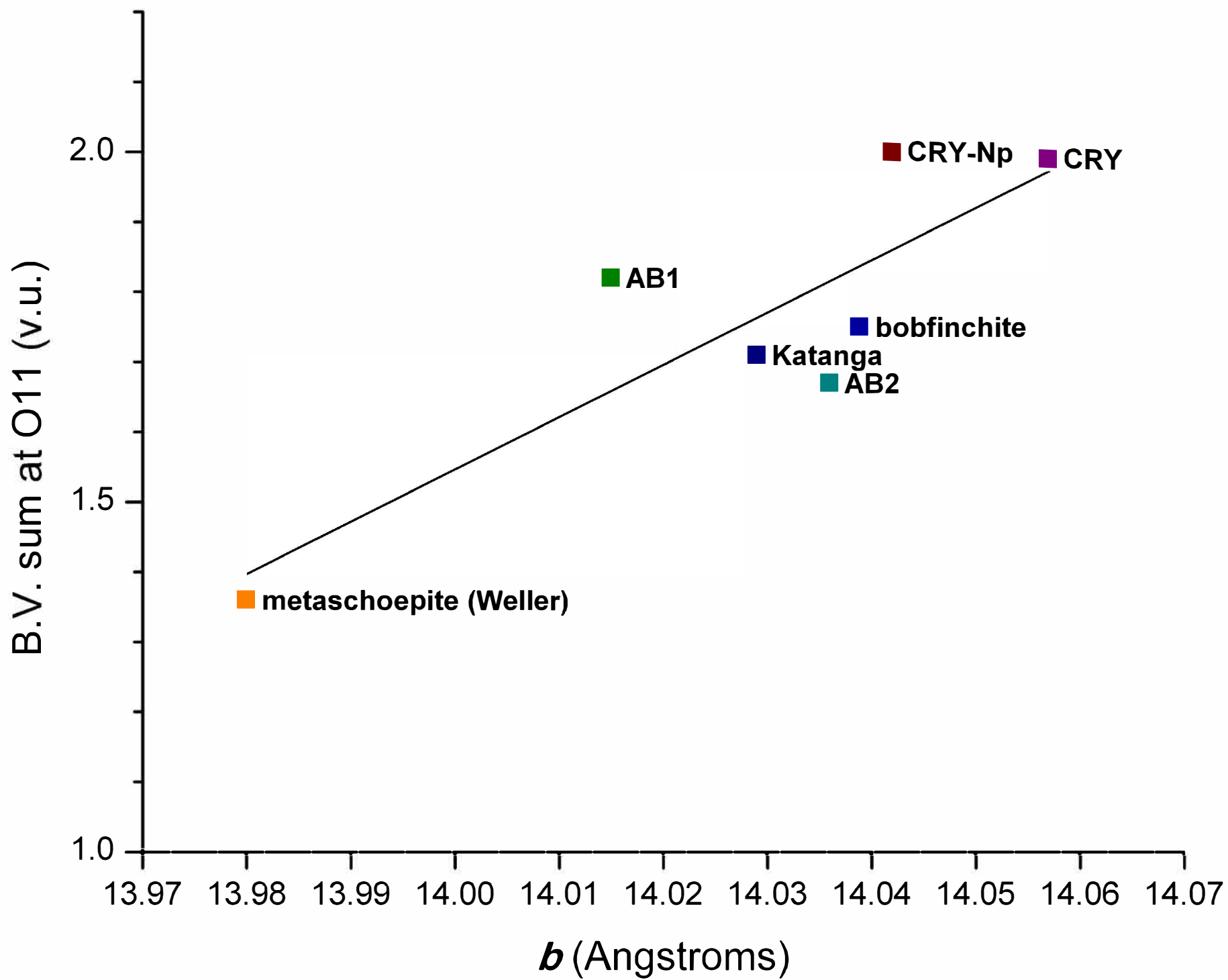
Na-rich metaschoepite and synthetic analog

Figure 6

Figure 7

Figure 8